Available online at www.sciencedirect.com
ScienceDirect
Trans. Nonferrous Met. Soc. China 27(2017) 352−362
Transactions of Nonferrous Metals Society of China
www.tnmsc.cn

Application of Ce−V/ sol−gel composite coating for corrosion protection of AM60B magnesium alloy

S. NEZAMDOUST, D. SEIFZADEH

Physical Chemistry Research Laboratory, Applied Chemistry Department,
Faculty of Basic Science, University of Mohaghegh Ardabili, Ardabil 5619911367, Iran

Received 13 February 2016; accepted 23 July 2016

Abstract: Application of a composite coating on AM60B magnesium alloy consisting of cerium−vanadium conversion coating and a hybrid sol−gel layer was investigated. Scanning electron microscopy and energy dispersive X-ray spectroscopy analyses revealed a cracked nodular structure for the cerium−vanadium conversion coating which was mainly composed of O, Ce, V, and Mg atoms. All the cracks in the conversion coating were completely sealed by a thin, compact and defect-free hybrid sol−gel film. Potentiodynamic polarization and electrochemical impedance spectroscopy experiments in Harrison's solution showed that the cerium−vanadium conversion coating provides minimal protection against corrosion while the composite coating significantly increases the corrosion resistance of the magnesium alloy. Sol−gel film provides protection against corrosion by sealing cracks in the cerium−vanadium conversion coating and acting as a barrier. Scanning electron microscopy analyses after polarization tests confirmed the results obtained by the electrochemical tests.

Key words: magnesium alloy; corrosion; conversion coating; sol−gel

1 Introduction

Widespread use of magnesium and its alloys is restricted due to their low corrosion resistance although they have many attractive properties such as high strength, low density (approximately 35% and 65% smaller than that of Al-based and Ti-based alloys respectively), high dimensional stability, suitable electromagnetic shielding characteristics, high stiffness, good machining, and high recycling ability [1−3]. Magnesium is active metal and a natural oxide film is formed on its surface in contact with the humid air. Unfortunately, the superficial oxide layer on the magnesium is loose and inherently porous and therefore, it is unable to provide a sufficient corrosion protection. Moreover, magnesium has very negative electrochemical potential and hence, the risk of galvanic corrosion (or bimetallic corrosion) is so high for magnesium in contact with the possible impurities or the secondary phases such as $Mg_{17}Al_{12}$, AlMn and Al_8Mn_5 [4]. Therefore, an especial surface treatment should be used before application of the magnesium alloys in any possible outdoor applications.

Conversion coating is one of the most popular surface treatment methods for the magnesium alloys due to low cost and operational simplicity. Another function of the conversion coatings is to provide strong adhesion between the metallic substrates and the subsequent organic or inorganic coatings. Traditional conversion treatments are performed in a bath containing chromium (VI) compounds. Unfortunately, hexavalent chromium ion has been found to be carcinogenic and therefore, there is a real necessity to find more environmentally-friendly alternatives. Different environmentally-acceptable conversion coatings based on the phytic acid [5], permanganate [6], phosphate [7−10], vanadium [11−13], Ti/Zr [14], molybdate and molybdate/ permanganate [15], molybdate/phosphate [16], and rare earth [17−19] have been studied on the magnesium alloys.

The formation mechanism and properties of cerium-based conversion coatings on the magnesium alloys have been widely investigated due to their good corrosion protection performance [20−30]. The cerium conversion coating with high corrosion resistance can be only obtained after long immersion time [25,31,32]. However, protective coatings may be obtained at shorter

Corresponding author: D. SEIFZADEH; Tel/Fax: +98-4533514702; E-mail: Seifzadeh@uma.ac.ir
DOI: 10.1016/S1003-6326(17)60039-6

immersion time by addition of hydrogen peroxide [20,33] and permanganate [34] to the cerium conversion coating bath. Unfortunately, stability of the cerium conversion coating bath decreases after addition of hydrogen peroxide. Also, permanganate-containing solutions are unworkable due to its rapid decomposition in acidic condition. Therefore, it is necessary to find new additives in order to obtain protective cerium conversion coatings. Recently, a new solution containing cerium nitrate and sodium metavanadate was introduced for application of cerium−vanadium (Ce−V) conversion coating on AZ31 magnesium alloy. It was found that the presence of sodium metavanadate causes the formation of polymeric vanadium hydroxide structure which is able to absorb the cerium and magnesium hydroxides and therefore shortening the plating time [31].

Despite the several advantageous of the conversion coatings, they can only provide limited stand-alone corrosion protection for the metallic substrates. In fact, the conversion coatings are inherently porous or cracked, so are not able to provide high corrosion protection performance without proper sealing (with suitable paints or resins). Sol−gel process is a chemical synthesis method based on the hydrolysis and condensation of the metal alkoxides (mostly organosilanes) and can be used to apply chemically stable and protective coatings on the metals via environmentally-friendly procedure. Sol−gel coatings show strong adhesion to the superficial oxides on the metallic substrates due to the formation of covalent M−O−Si bonds [35,36]. The conversion coatings are generally composed of mixed oxide films with cracked or porous structure and hence, a sol−gel film may be attached to the conversion coatings either by the mechanical interlocking (due to the presence of numerous cracks or micro cracks on the conversion coating structure) or chemical bonding (between the sol−gel coating and mixed oxides of the conversion film). Therefore, the sol−gel films may be suitable candidates to use as seal coatings in order to increase the corrosion resistance of the conversion coatings on the magnesium alloys. Introduction of an organo-modified silane precursor to an inorganic sol−gel system makes the obtained film more compatible to subsequent organic top coats. Therefore, the application of a hybrid (organic/inorganic) sol−gel coating may provide new possibilities to apply future paint or resins on the magnesium alloys to reach the maximum corrosion protection [35].

On the other hand, direct application of adherent and corrosion protective sol−gel film on the magnesium alloys is not possible mainly due to reaction between the active magnesium substrate and the acidic sol solution which leads to the formation of loose sol−gel layer with insufficient adherence. The adhesion and corrosion protection of a sol−gel film on the magnesium substrates can be substantially improved by application of a suitable conversion coating pretreatment [37].

Based on the above-mentioned facts, it seems that the conversion coating/sol−gel composites have better corrosion protection and stronger adherence than the single conversion or sol−gel coatings, respectively. There is limited information in the literature about the application of the conversion coating/sol−gel composites on the magnesium alloys. However, this idea has been previously investigated by at least two research groups. MURILLD-GUTIERREZ et al [38] has investigated the corrosion resistance of a composite coating consisting of a phosphate conversion layer and an organic-inorganic hybrid sol−gel film on Elektron21 magnesium alloy in 0.05 mol/L NaCl solution. It was found that the composite coating shows better corrosion protection performance than the single conversion coating. Also, the application and properties of a composite coating based on the molybdate conversion film and a hybrid sol−gel layer on AZ91D magnesium alloy has been investigated by HU et al [39]. The results showed that the composite coating considerably increases the corrosion resistance of the AZ91D magnesium alloy.

The aim of this study was to investigate the application of new and environmentally-friendly composite coating on AM60B magnesium alloy for corrosion protection. First, the Ce−V conversion coating [31] was applied by the solution containing cerium nitrate and sodium metavanadate. Afterwards, hybrid organic−inorganic sol−gel film based on tetraethylorthosilicate (TEOS) and 3-Glycidoxypropyl-trimethoxysilane (GPTMS) deposited on the conversion coating to achieve a higher level of the corrosion protection. Surface analysis of the alloy samples after application of the conversion and composite coatings was conducted by the scanning electron microscopy (SEM) and energy dispersive X-ray spectroscopy (EDS). The corrosion behavior of the single conversion coating together with the composite coating was investigated with potentiodynamic polarization and electrochemical impedance spectroscopy (EIS) methods.

2 Experimental

2.1 Substrate

The substrate samples with dimensions of 50 mm × 15 mm × 2 mm were prepared from the AM60B magnesium alloy bar. The chemical composition of the alloy samples was determined by the EDS method which mainly contained 6.33% Al, 0.68% Zn, 0.24% Mn, and Mg balance (mass fraction). The samples were polished with emery papers (No. 100 to 1000) and then rinsed

with distilled water. Finally, the samples were cleaned ultrasonically in acetone at 40 °C for 15 min before being immersed in the conversion coating bath immediately.

2.2 Ce−V conversion coating

The pretreated alloy samples were immersed in 250 mL of the conversion coating solution containing 4 g/L $Ce(NO_3)_2·6H_2O$ and 2.4 g/L $NaVO_3$ at 80 °C for 30 min. The pH of the conversion coating bath was adjusted to 2.5 by addition of HNO_3.

2.3 Composite coating

The sol−gel solution was prepared by mixing 0.04 mol TEOS, 0.02 mol GPTMS and 1.23 mol acidic water (hydrochloric acid with pH~1.5) so that the molar ratio of the water molecules to alkoxide groups was about 5:1. The mixture was vigorously stirred (700 r/min) by a magnetic stirrer for about 30 min at laboratory temperature (~23 °C). The alloy samples which were primarily treated in the conversion bath were then immersed in the sol−gel solution for 5 min. Then, the samples were withdrawn using the dip-coater instrument with a constant speed of 50 mm/min. Afterwards, the samples were kept at 60 °C for about 2 h in a digital furnace (Pars Azma Co.) to slow evaporation of the residual water in order to avoid the crack formation. Finally, the samples were subjected to the heat treatment at 130 °C for about 1 h. Temperature of the digital furnace was increased at a constant rate of 2 °C/min to avoid the possible crack formation due to the difference in thermal expansion coefficients of the sol−gel layer and the alloy substrate.

2.4 Coating characterization

Fourier transform infrared (FTIR) spectra were obtained for the original organosilane precursors together with the synthesized sol before and after the heat treatment using Perkinelmer spectrum RX instrument. Also, a SEM instrument (LEO, VP 1430) at high vacuum and 15 kV EHT was used to study the surface and cross-sectional morphologies of both the conversion film and composite coating. In addition, the morphology of the bare and coated alloy samples after polarization corrosion tests were examined by SEM. Moreover, the EDX (RÖNTEC GmbH, Germany) method was used to determine the chemical composition of the alloy sample before and after application of the conversion coating.

2.5 Corrosion tests

Potentiodynamic polarization and EIS corrosion tests were conducted with a potentiostat-galvanostat (μautolab3) supported by the Nova 1.6 software in the Harrison's solution (0.35% ammonium sulfate and 0.05% sodium chloride) at laboratory temperature (~23 °C). A classic electrochemical cell consisting of working, counter and reference electrodes was used. The alloy samples were firstly embedded in mounting epoxy resin leaving a working area of 1 cm^2 and then were used as working electrodes. Also, a platinum sheet (with surface area of 1 cm^2) and a saturated Ag−AgCl electrode were used as counter and reference electrodes, respectively. The EIS tests were carried out using sine wave of 10 mV amplitude across the frequency range between 100 kHz and 100 mHz at the open circuit potential. Before the EIS tests, the alloy samples were immersed in the corrosive solution for about 10 min to establish the steady state corrosion potential. In order to record the polarization curves, the potential of the working electrodes was scanned around the corrosion potential (φ_{corr}) with a scan rate of 1 mV/s. The polarization tests were performed immediately after the EIS measurements. The corrosion tests were also carried out by the uncoated bare alloy to compare its results with the coated samples. The bare sample was firstly polished with emery papers, rinsed with distilled water and finally degreased in ethanol before being immersed in the corrosive solution. Each electrochemical test was repeated at least three times and the similar results were obtained. The volume of the corrosive solution for each electrochemical test was about 200 mL and all experiments were carried out under ambient pressure without any stirring.

3 Results and discussion

3.1 Conversion coating

Surface morphology of the alloy sample after Ce−V conversion coating treatment is presented in Fig. 1 at low (a) and high (b) magnifications. Also, Fig. 1(c) shows the cross-sectional morphology of the Ce−V treated alloy sample.

The conversion coating showed cracked structure which may be related to the evolution of gas product due to corrosion of the alloy surface. It is obvious that the cracked layer is composed of a nodular structure with relatively uniform distribution of nodule size (Fig. 1(b)). Also, it is clear from the cross-sectional SEM image (Fig. 1(c)) that the Ce−V conversion coating with the thickness less than 1 μm is firmly embedded on the alloy surface so that the interface between the conversion coating and the magnesium alloy is hardly distinguishable. JIANG et al [31] studied the formation mechanism of the Ce−V conversion film in sufficient details. However, the related mechanism can be briefly explained here. The conversion coating bath is acidic and hence it is so corrosive for the electrochemically active magnesium alloy. Therefore, the rapid corrosion process

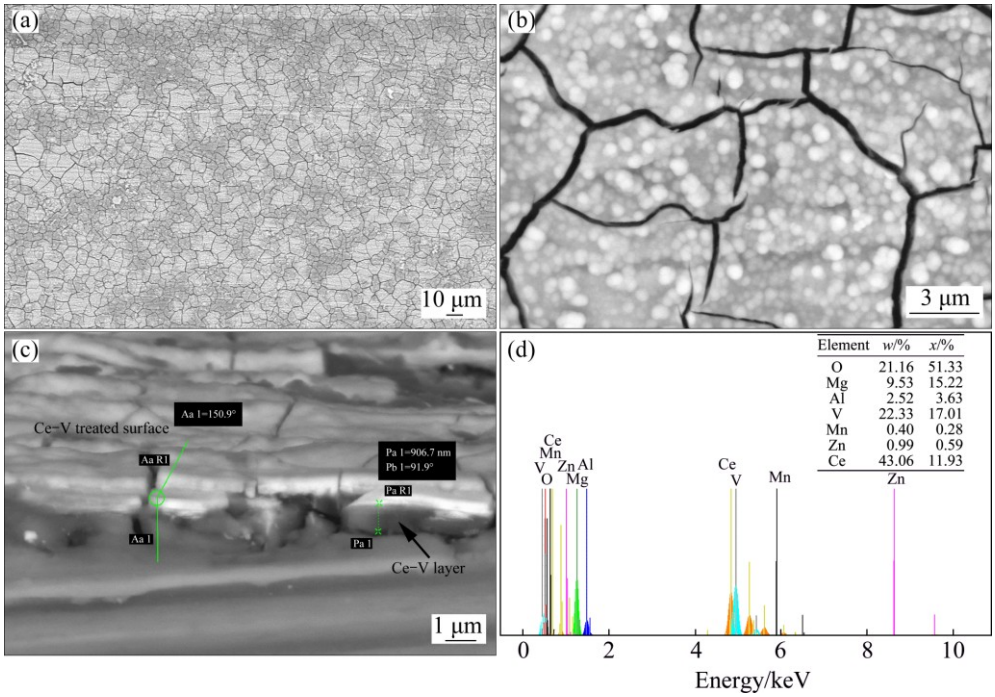

Fig. 1 Surface morphology of Ce−V conversion coating at low (a) and high (b) magnifications, its cross-sectional morphology (c), and EDS spectrum (d)

of the alloy substrate starts immediately after immersion:

$$Mg \rightarrow Mg^{2+}+2e \quad (1)$$

$$2H_2O+2e \rightarrow H_2+2OH^- \quad (2)$$

In Eq. (1), only the anodic oxidation of the Mg is given, but it is clear that the anodic dissolution of other alloying elements such as aluminium is also possible. The fast corrosion of the alloying elements makes the metal/electrolyte interface so alkaline and then hydroxides of the alloying elements are precipitated. Also, Ce^{3+} ions react with the produced hydroxyl ions to create initial crystal nucleus of the cerium hydroxide on the alloy surface. Afterward, the nucleation centres of the cerium hydroxide grow to cover the alloy surface. Simultaneously, VO_2^+ cation (which is the predominant form of the vanadium in a sodium metavanadate solution when the concentration is 2.4 g/L and the pH is 2.5) reacts with water to produce vanadium hydroxides on the alloy surface:

$$VO_2^+ +2H_2O \rightarrow VO(OH)_3+H^+ \quad (3)$$

$$VO(OH)_3+2H_2O \rightarrow VO(OH)_3+(OH_2)_2 \quad (4)$$

The vanadium hydroxides are not stable in the bath condition and their spontaneous polymerization takes place to form stable polymeric structure with V(V) — O — V(V) linkages. It is believed that this polymeric structure is able to adsorb or capture the other hydroxides before they grow up. Therefore, all of the hydroxides simultaneously deposit on the alloy surface to form a conversion film. During the drying process, the metallic hydroxides dehydrate to form the corresponding oxides. Dehydration may be another reason for the formation of cracked conversion film. It is previously reported that the pH value at the interfacial zone affects the formation process of the hydroxides, so that vanadium hydroxide is deposited as soon as the pH value is changed at the interface and then, cerium hydroxide is formed with other hydroxides after formation of more hydroxyl ions. Therefore, the Ce−V conversion coating is composed of an inner layer which mainly contained vanadium hydroxides/oxides and an outer layer containing both vanadium and the other hydroxides/oxides.

In this work, EDS analysis was performed to study the chemical composition of the Ce−V conversion coating. The related spectra together with the results of the quantitative analysis are given in Fig. 1(d). It is found that the conversion film is mainly composed of O, V, Ce, Mg, Al, Zn, and Mn atoms and therefore, the above-mentioned mechanism can be acceptable.

3.2 Composite coating

3.2.1 FTIR

The FTIR spectra of the original precursors are given in Fig. 2. Characteristic IR absorbance peaks of the TEOS related to C—H rocking (CH_3) at 965.9 and 1169.6 cm^{-1}, symmetric C — H bending (CH_3) at 1391.5 cm^{-1}, asymmetric C — H stretching (CH_3) at 2893.6 and 2977.1 cm^{-1}, asymmetric C—H stretching

(CH_2) at 2929.7 cm^{-1}, and asymmetric C—O stretching at 1107.9 cm^{-1} can be found in the spectrum [40]. Two strong vibrational peaks in the FTIR spectrum of the GPTMS located at 1092.2 and 1194.9 cm^{-1} are related with waging vibrations of CH_2 in propyl chain and glycidoxy group, respectively [41] while the peak at around 909.9 cm^{-1} is related to pure vibrations of the epoxy ring [42]. Also the peak at 1254.1 cm^{-1} is due to vibration of the epoxy group in GPTMS [43]. Moreover, two bands observed in the FTIR spectrum of the GPTMS at 2943.3 and 2841.4 cm^{-1} are assigned to the CH_3 stretching modes of the OCH_3 groups [42].

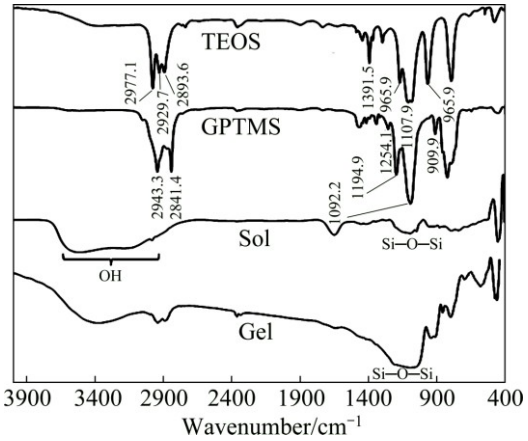

Fig. 2 FTIR spectra of original TEOS and GPTMS precursors along with FTIR spectra of hydrolyzed sol and cured gel

The FTIR spectra of the hybrid sol (after hydrolysis under acidic condition) and the final gel powder (after curing in digital furnace) were also recorded in order to follow the structural changes during the sol−gel process (Fig. 2). There are some important differences between the obtained FTIR spectra with those obtained for the organosilane precursors. Most of the characteristic peaks of the TEOS and GPTMS disappeared (or significantly weakened) after hydrolysis and a broad peak from 3000 to 3600 cm^{-1} appeared which was related to the SiOH group, unused water molecules and produced alcohols. The broad vibrational peak at around 1100 cm^{-1} in the FTIR spectrum of the hydrolyzed sol was due to the transforming from Si—OH to Si—O—Si indicating that the condensation reactions started even before the completion of the hydrolysis [43]. The intensity of the broad peak at around 1100 cm^{-1} corresponding to the asymmetric stretching vibrations of Si—O—Si was strongly increased in the case of the cured gel due to the promotion of the condensation reactions.

3.2.2 Surface and cross-sectional morphology

The corrosion protection performance of a coating strongly depends on its morphology and thickness. So, the SEM instrument was used to study the surface and cross-sectional morphologies of the applied composite coating. The surface morphologies of the composite Ce−V/sol−gel coating are shown in Fig. 3 at low (a) and high (b) magnifications. It is obvious that the conversion coating was completely covered by a smooth and compact sol−gel film. There is no defect such as cracks or pores on the surface of the composite coating. Also, Fig. 3(c) shows the cross-sectional morphology of the composite coating. It is evident that the sol−gel film was strongly attached to the conversion coating and there is no defect or crack at the sol−gel/conversion coating interface. The sol−gel film can be attached to the alloy surface by diffusion in the pores and cracks of the Ce−V conversion coating. Also, the sol−gel layer may be chemically bonded with the conversion coating via formation of Ce—O—Si, V—O—Si, and Mg—O—Si bonds. The thickness of the sol−gel film is more than 1 μm while the thickness of the composite coating is near to 2 μm. Strong adhesion of the sol−gel film to the conversion coating (and therefore to the alloy substrate) provides more possibilities to apply corrosion resistant and adherent organic resins on the magnesium alloy as mentioned above [35].

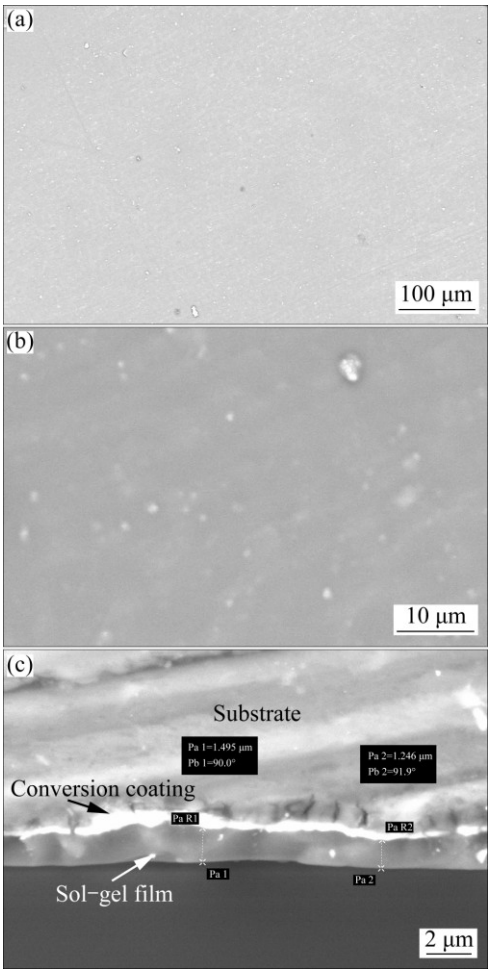

Fig. 3 Surface morphology of composite coating at low (a) and high (b) magnifications and its cross-sectional morphology (c)

3.2.3 Corrosion tests

Based on the morphological studies, better corrosion protection performance for the Ce−V/sol−gel composite was expected compared with the single conversion coating. This idea was examined by the electrochemical methods including potentiodynamic polarization and EIS experiments in Harrison's solution at room temperature. Also, the appearance photos and SEM images were taken from the surface of the bare, conversion coating and composite coating after polarization corrosion tests to validate the results.

Representative potentiodynamic polarization curves of the conversion and composite coatings are shown in Fig. 4. The polarization curve for a freshly pretreated bare alloy sample was also included to compare its results with those obtained for the conversion and composite coatings. It can be seen that the anodic and cathodic current of the alloy sample with conversion layer is lower than that of the bare alloy at all the applied over-potentials. However, the observed difference is not significant indicating that the conversion coating provides only partial protection for the magnesium against corrosion. The corrosion protection of the conversion coating is related with the formation of mixed oxide layer on the alloy surface which reduces the available area for the anodic and cathodic reactions and delays the transportation of corrosive species, thereby inhibiting the corrosion process.

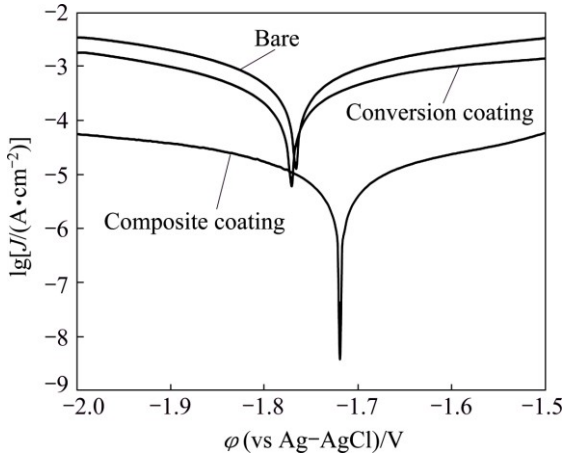

Fig. 4 Potentiodynamic polarization curves of bare alloy, conversion coating and composite coating in Harrison's solution

In contrast to the conversion coating, composite coating showed much lower anodic and cathodic currents meaning that it is able to significantly increase the corrosion resistance of the alloy sample. The polarization parameters including the corrosion potential (φ_{corr}), anodic and cathodic Tafel slopes (b_a and b_c respectively), and corrosion current density (J_{corr}) were obtained by the Tafel extrapolation method (Table 1). The composite coating showed much lower J_{corr} and nobler φ_{corr} than the Ce−V conversion coating indicating that it has much better corrosion protection. The composite coating exhibited a corrosion current density more than 31 and 67 times lower than the conversion coating and bare alloy, respectively. These results indicate that the sol−gel film is able to fill all the possible cracks or pores in the Ce−V conversion coating to provide much better protection against corrosion. Moreover, application of the future sol−gel film increases the thickness of the coating which has a direct effect on its corrosion protection performance.

Table 1 Polarization parameters for bare, conversion coating and composite coating

Sample	φ_{corr} (vs Ag−AgCl)/V	b_a/ (mV·dec^{-1})	$-b_c$/ (mV·dec^{-1})	J_{corr}/ (μA·cm^{-2})
Bare	−1.765	151	129	310.9
Conversion coating	−1.770	144	123	145.8
Composite coating	−1.718	140	136	4.6

Electrochemical impedance spectroscopy was also used as powerful complementary method to validate the results obtained by the polarization curves. Figure 5 shows the impedance response of the bare alloy, conversion coating and composite coating in Harrison's solution at different forms including Nyquist (a), bode modulus (b) and phase bode (c) plots. The Nyquist plot for the bare alloy shows two small capacitive semicircles at high and intermediate frequencies followed by an inductive loop in low frequencies. The capacitive semicircle at high frequencies is generally related to the charge transfer at the substrate/electrolyte interface while the other capacitive loop at intermediate frequencies is due to the formation of partially protective and porous oxide/hydroxide film on the alloy surface. Also, the presence of the inductive loop at low frequencies may be related to the pitting initiation [44−46]. The shape of the impedance response was not changed after application of both the conversion and composite coatings, but the size of the semicircles was significantly increased. This effect is more pronounced for the composite coating, indicating that it has much better corrosion protection performance. Quantitative results were obtained by fitting the experimental EIS data to an appropriate equivalent circuit (Fig. 5(d)). In this model, R_s, R_{ct}, and R_f are considered to account for the resistances of the solution, charge transfer and surface film, respectively. Also, two constant phase elements (CPE) including CPE_{dl} and CPE_f are used in the equivalent circuit to model the capacitive behavior of the electrical double layer and surface film, respectively. In this model, CPE elements are used

instead of the ideal capacitor elements to account for the non-ideal behavior arising due to surface heterogeneity and roughness [47]. The impedance of CPE element can be modeled by [48]

$$Z_{CPE}=1/Q(j\omega)^n \quad (5)$$

where Q, ω and j are the CPE constant, angular frequency, and imaginary number, respectively. The factor n is CPE exponent range between 0 and 1 which can be regarded as an index of deviation from the ideal capacitor behavior.

Moreover, an inductor (L) and resistance (R_L) elements were inserted in the circuit to model the inductive behavior. Fitting was carried out by Zview2 software and the quantitative impedance parameters were calculated (Table 2). The results of data fitting are also superimposed on the Nyquist plots as solid lines. The small increase in the R_{ct} and R_f is observed for the alloy sample after treatment with the conversion bath indicating a partial corrosion protection of the conversion coating. Despite the sample treated with the conversion coating, a significant increasing in the R_{ct} and R_f was observed for the alloy sample coated with the composite coating. This indicates that the corrosion protection performance of the conversion coating significantly increases after sealing with the sol−gel layer. These results are in good agreement with those obtained by the polarization measurements. Also, it is obvious that the values of the CPE_{dl} and CPE_f are significantly decreased after the application of the composite coating. The decreasing of these values is due to the sealing of the defects by sol−gel film which hinders the diffusion of

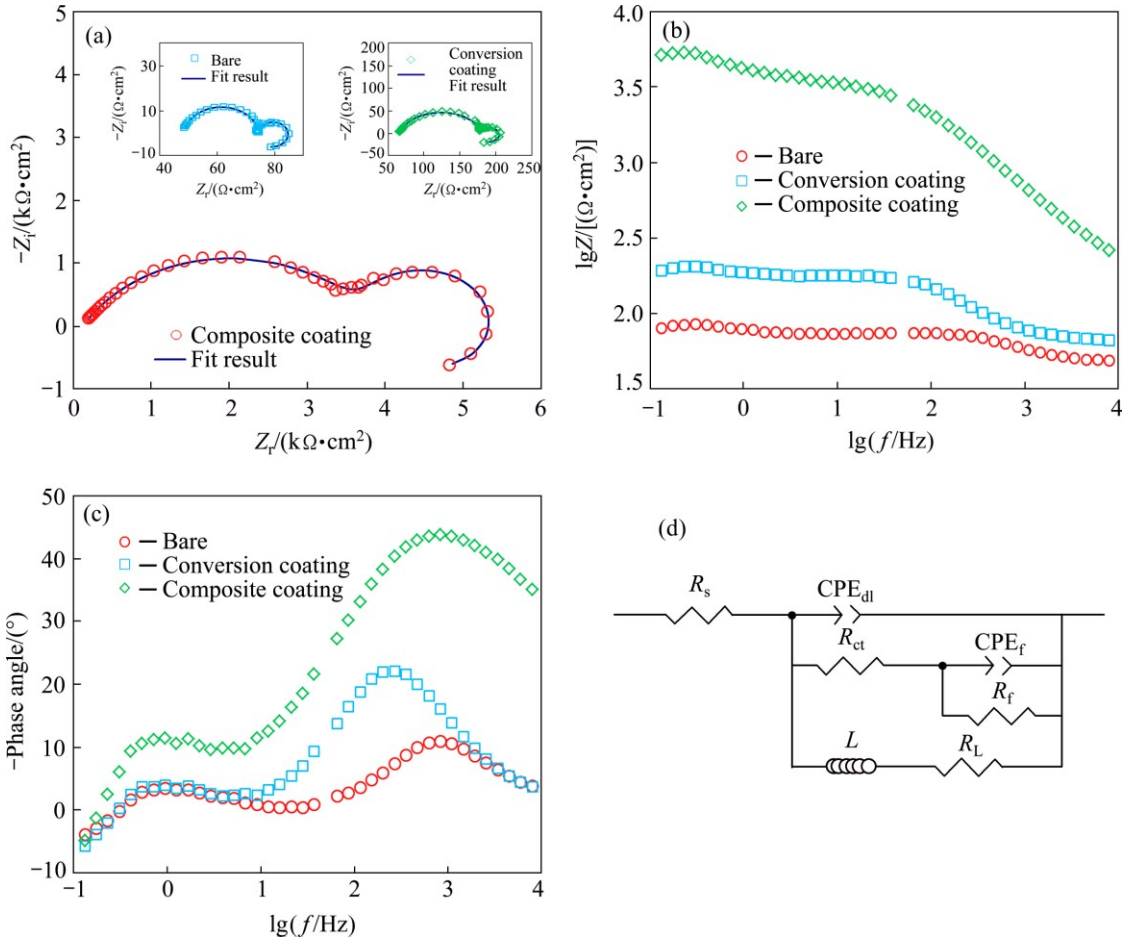

Fig. 5 Nyquist (a), bode modulus (b) and phase bode (c) plots of bare alloy, conversion coating and composite coating in Harrison's solution together with appropriate equivalent circuit (d)

Table 2 Quantitative impedance parameters for bare, conversion coating and composite coating

Sample	$CPE_{dl}/(\mu S^n\cdot\Omega^{-1}\cdot cm^2)$	n_{dl}	$R_{ct}/(\Omega\cdot cm^2)$	$CPE_f/(mS^n\cdot\Omega^{-1}\cdot cm^2)$	n_f	$R_f/(\Omega\cdot cm^2)$	$R_L/(\Omega\cdot cm^2)$	$L/(kH\cdot cm^2)$
Bare	16.54	0.9222	21.4	19.13	0.9955	13.5	35.8	0.123
Conversion	21.92	0.8666	114.5	9.17	0.9988	40.1	295.0	0.502
Composite	4.45	0.6635	3750.0	0.18	0.9627	2246.0	11148	21.66

water molecule in the composite film or in the double layer structure.

Figure 6(a) shows the appearance of the bare and coated samples after polarization test. Also, the appearance of the bare alloy, conversion coating, and composite coating before and after polarization tests was compared in Figs. 6(b)−(d) respectively.

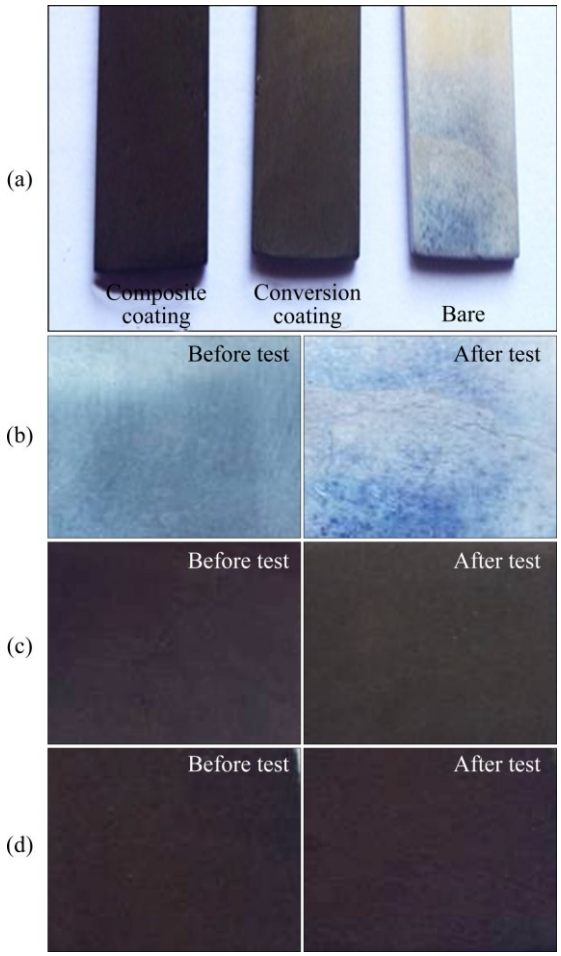

Fig. 6 Appearance photos of bare and coated sample after polarization test (a) together with comparative photos before and after polarization tests for bare alloy (b), conversion coating (c), and composite coating (d)

The effects of the corrosion after polarization test is obvious on the bare alloy surface due to its low corrosion resistance. Detection of the corrosion damages on the surface of the coated samples (Figs. 6(c) and (d)) was difficult due to dark brown to black appearance of the coatings. However, there were no detectable macroscopic pores or cracks on the composite coated sample after polarization test and it can be seen that the surface of the composite coating has remained unchanged after polarization test indicating its good anticorrosion performance.

Surface morphology of the samples after corrosion tests was also investigated by SEM. Figures 7(a) and (b) show the surface morphology of the bare alloy sample after polarization test at low and high magnifications, respectively. The bare AM60B alloy was severely damaged in Harrison's solution mainly due to the application of large anodic polarization. It is well known that the AM60 alloy is mainly composed of primary crystallized α phase (magnesium-rich) and eutectic phase consisting of α-phase and aluminum-rich β-phase ($Mg_{17}Al_{12}$) [49]. It seems that the island-like area in the SEM image of the bare alloy is β-phase while the rest area is α-Mg since the electrochemical activity of the magnesium is much more than aluminum. Formation of cracks (Fig. 7(b)) on the surface of the bare alloy sample may be related to the rapid evolution of hydrogen gas bubbles during the cathodic polarization. Also, the rapid formation of hydrogen gas bubbles was observed during the anodic polarization of the bare alloy more probably due to negative difference effect [50]. Figures 7(c) and (d) show that the anodic dissolution of the alloy sample with conversion coating was significantly reduced compared with the bare alloy but there are still considerable amount of corrosion damages on the surface. It is well-known that heavy elements strongly backscatter electrons; hence the areas with those elements appear brighter in the SEM image while the lighter elements tend to absorb electrons and thus appear darker. Therefore, the darker areas on the SEM images are magnesium-rich areas which were more severely damaged by anodic dissolution compared with the brighter area. The SEM image of the sample coated with composite coating after corrosion tests (Figs. 7(e) and (f)) was completely different. There is still a stable sol−gel film on the alloy sample even after polarization test indicating acceptable corrosion protection of the applied composite film. Also, existence of the stable sol−gel layer on the alloy without detaching from the surface shows that the applied film is adherent more probably due to mechanical interlocking and chemical bonding between the sol−gel coating and conversion coating. However, there are some pores in the composite coating indicating the localized nature of the corrosion process. This result may be arising from the non-conducting future of the sol−gel layer which concentrates all the anodic currents on the weak sites of the composite coating leading to formation of pores.

4 Conclusions

1) The Ce−V conversion coating on AM60B magnesium alloy showed a cracked structure composed of nodules with relatively uniform size distribution.

2) EDS analysis showed that the Ce−V conversion coating is mainly composed of O, V, Ce, Mg, Al, Zn, and Mn atoms.

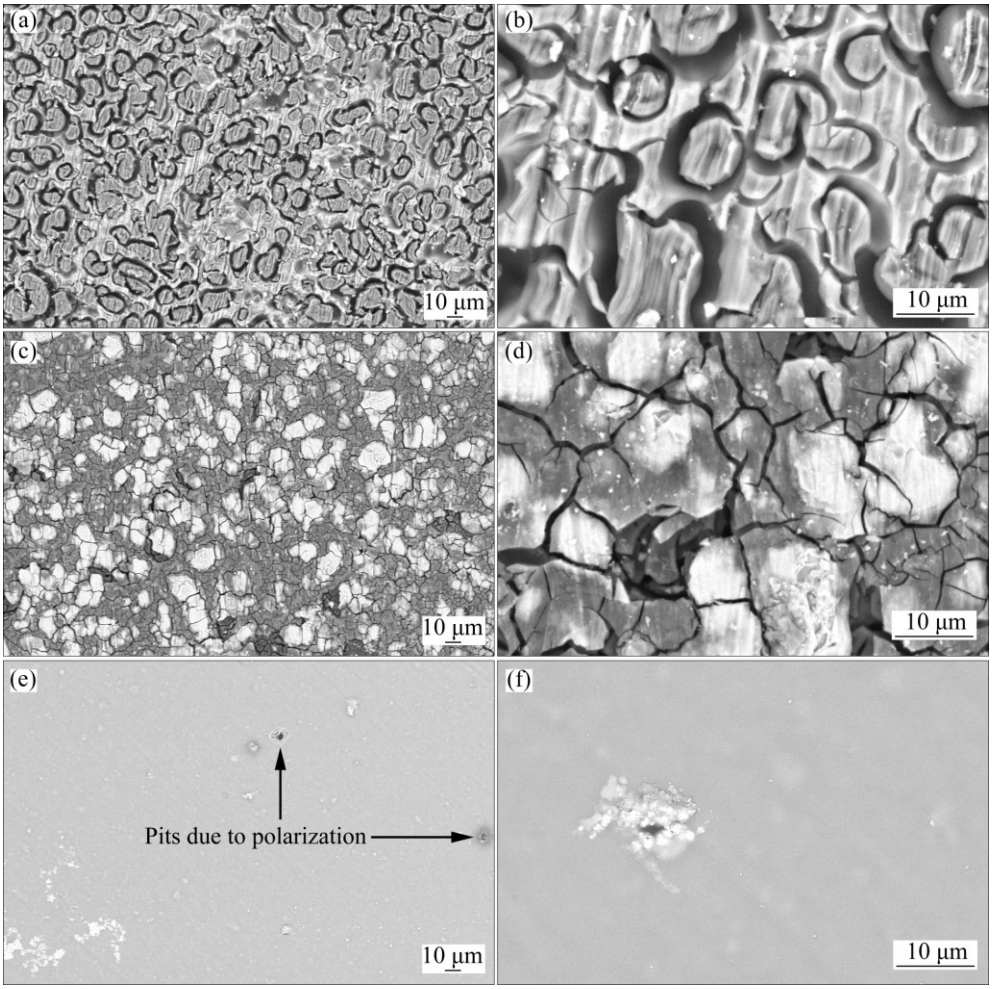

Fig. 7 Surface morphologies of bare (a, b), conversion coating (c, d), and composite coating (e, f) after polarization tests at two different magnifications

3) SEM observation of the composite coating showed that the cracks of the Ce−V conversion coating was completely covered by a smooth, compact, and defect-free sol−gel film. Cross-sectional SEM image of the composite coating revealed that the sol−gel layer was strongly attached to the conversion coating.

4) Potentiodynamic polarization tests showed that the corrosion current densities of the composite coating in Harrison's solution were approximately 31 and 67 times lower than those obtained for the bare alloy with and without application of the conversion coating respectively.

5) A significant increasing in the R_{ct} and R_f was observed for the alloy sample after application of the composite coating with respect to the bare alloy before and after the conversion coating treatment. Also, the CPE_{dl} and CPE_f were significantly decreased after application of the composite coating due to the sealing of the defects by sol−gel film which hinders the diffusion of water molecule.

6) SEM images after polarization tests confirmed much better corrosion protection of the composite coating compared with the conversion coating.

References

[1] SHANG W, CHEN B, SHI X, CHEN Y, XIAO X. Electrochemical corrosion behavior of composite MAO/sol-gel coatings on magnesium alloy AZ91D using combined micro-arc oxidation and sol−gel technique [J]. Journal of Alloys and Compounds, 2009, 474: 541−545.

[2] GRAY J E, LUAN B. Protective coatings on magnesium and its alloys—A critical review [J]. Journal of Alloys and Compounds, 2002, 336: 88−113.

[3] CUI Xue-jun, YANG Rui-song, LIU Chun-hai, YU Zu-xiao, LIN Xiu-zhou. Structure and corrosion resistance of modified micro-arc oxidation coating on AZ31B magnesium alloy [J]. Transactions of Nonferrous Metals Society of China, 2016, 26: 814−821.

[4] WATITON C A, MARTN H J, HORSTEMERYER M F, WA P T. Quantification of corrosion mechanisms under immersion and salt-spray environments on an extruded AZ31 magnesium alloy [J]. Corrosion Science, 2012, 56: 194−208.

[5] ZHANG R, CAI S, XU G, ZHAO H, LI Y, WANG X, HUANG K, REN M, WU X. Crack self-healing of phytic acid conversion coating on AZ31 magnesium alloy by heat treatment and the corrosion

resistance [J]. Applied Surface Science, 2014, 313: 896−904.
[6] JIAN Shun-yi, CHU Yu-ren, LIN Chao-sung. Permanganate conversion coating on AZ31 magnesium alloys with enhanced corrosion resistance [J]. Corrosion Science, 2015, 93: 301−309.
[7] ZENG Rong-chang, ZHANG Fen, LAN Zi-dong, CUI Hong-Zhi, HAN En-hou. Corrosion resistance of calcium-modified zinc phosphate conversion coatings on magnesium–aluminium alloys [J]. Corrosion Science, 2014, 88: 452−459.
[8] PHUONG N V, MOON S. Comparative corrosion study of zinc phosphate and magnesium phosphate conversion coatings on AZ31 Mg alloy [J]. Materials Letter, 2014, 122: 341−344.
[9] ZHAO M, LI J, HE G, XIE H, FU Y. An investigation of the effect of a magnetic field on the phosphate conversion coating formed on magnesium alloy [J]. Applied Surface Science, 2013, 282: 499−505.
[10] ZENG Rong-chang, HU Yan, ZHANG Fen, HUANG Yuan-ding, WANG Zhen-lin, LI Shuo-qi, HAN En-hou. Corrosion resistance of cerium-doped zinc calcium phosphate chemical conversion coatings on AZ31 magnesium alloy [J]. Transactions of Nonferrous Metals Society of China, 2016, 26: 472−483.
[11] LI K, LIU J, LEI T, XIAO T. Optimization of process factors for self-healing vanadium-based conversion coating on AZ31 magnesium alloy [J]. Applied Surface Science, 2015, 353: 811−819.
[12] NIU L, CHANG S H, TONG X, LI G, SHI Z. Analysis of characteristics of vanadate conversion coating on the surface of magnesium alloy [J]. Journal of Alloys and Compounds, 2014, 617: 214−218.
[13] YANG K H, GER M D, HWU W H, SUNG Y, LIU Y C. Study of vanadium-based chemical conversion coating on the corrosion resistance of magnesium alloy [J]. Materials Chemistry and Physics, 2007, 101: 480−485.
[14] YI A, DU J, WANG J, MU S, ZHANG G, LI W. Preparation and characterization of colored Ti/Zr conversion coating on AZ91D magnesium alloy [J]. Surface and Coatings Technology, 2015, 276: 239−247.
[15] WANG G, ZHANG M, WU R. Molybdate and molybdate/ permanganate conversion coatings on Mg−8.5Li alloy [J]. Applied Surface Science, 2012, 258: 2648−2654.
[16] YONG Z, ZHU J, QIU C, LIU Y. Molybdate/phosphate composite conversion coating on magnesium alloy surface for corrosion protection [J]. Applied Surface Science, 2008, 255: 1672−1680.
[17] LIN C, CHANGGUO C, NINGNING W, JIMIN W, LING D. Study of cerium and lanthanum conversion coatings on AZ63 magnesium alloy surface [J]. Rare Metal Materials and Engineering, 2015, 44: 333−338.
[18] YANG X, WANG G, DONG G, GONG F, ZHANG M. Rare earth conversion coating on Mg−8.5Li alloys [J]. Journal of Alloys and Compounds, 2009, 487: 64−68.
[19] RUDD A L, BRESLIN C B, MANSFELD F. The corrosion protection afforded by rare earth conversion coatings applied to magnesium [J]. Corrosion Science, 2000, 42: 275−288.
[20] CHEN Dong-chu, WU Jian-feng, LIANG Yi-qing, YE Shu-lin, LI Wen-fang. Preparation of cerium oxide based environment-friendly chemical conversion coating on magnesium alloy with additives [J]. Transactions of Nonferrous Metals Society of China, 2011, 21: 1905−1910.
[21] DABALA M, BRUNELLI K, NAPOLITANI E, MAGRINI M. Cerium-based chemical con-version coating on AZ63 magnesium alloy [J]. Surface and Coatings Technology, 2003, 172: 227−232.
[22] ARDELEAN H, FRATEUR I, MARCUS P. Corrosion protection of magnesium alloys by cerium, zirconium and niobium-based conversion coatings [J]. Corrosion Science, 2008, 50: 1907−1918.
[23] LI L, LEI J, YU S, TIAN Y, JIANG Q, PAN F. Formation and characterization of cerium conversion coatings on magnesium alloy [J]. Journal of Rare Earths, 2008, 26: 383−387.
[24] CUI X, YANG Y., LIU E, JIN G, ZHONG J, LI Q. Corrosion behaviors in physiological solution of cerium conversion coatings on AZ31 magnesium alloy [J]. Applied Surface Science, 2011, 257: 9703−9709.
[25] MONTEMOR M F, SIMOES A M, FERREIRA M G S, CARMEZIM M J. Composition and corrosion resistance of cerium conversion films on the AZ31 magnesium alloy and its relation to the salt anion [J]. Applied Surface Science, 2008, 254: 1806−1814.
[26] GAO H F, TAN H Q, LI J, WANG Y Q, XUN J Q. Synergistic effect of cerium conversion coating and phytic acid conversion coating on AZ31B magnesium alloy [J]. Surface and Coatings Technology, 2012, 212: 32−36.
[27] SUN J, WAN G. Preparation and corrosion resistance of cerium conversion coatings on AZ91D magnesium alloy by a cathodic electrochemical treatment [J]. Surface and Coatings Technology, 2014, 254: 42−48.
[28] BRUNELLI K, DABALA M, CALLIARI I, MAGRINI M. Effect of HCl pre-treatment on corrosion resistance of cerium-based conversion coatings on magnesium and magnesium alloys [J]. Corrosion Science, 2005, 47: 989−1000.
[29] WANG C, ZHU S, JIANG F, WANG F. Cerium conversion coatings for AZ91D magnesium alloy in ethanol solution and its corrosion resistance [J]. Corrosion Science, 2009, 51: 2916−2923.
[30] LIN C S, FANG S K. Formation of cerium conversion coatings on AZ31 magnesium alloys [J]. Journal of the Electrochemical Society B, 2005, 152: 54−59.
[31] JIANG X, GUO R, JIANG S. Microstructure and corrosion resistance of Ce−V conversion coating on AZ31 magnesium alloy [J]. Applied Surface Science, 2015, 341: 166−174.
[32] MONTERNOR M F, SIMOES A M, CARMEZIM M J. Characterization of rare-earth conversion films formed on the AZ31 magnesium alloy and its relation with corrosion protection [J]. Applied Surface Science, 2007, 253: 6922−6931.
[33] SCHOLES F H, SOSTE H C, HUGHES A E, HARDIN S G, CURTIS P R. The role of hydrogen peroxide in the deposition of cerium-based conversion coatings [J]. Applied Surface Science, 2006, 253: 1770−1780.
[34] ZHENG R F, LIANG C H. Conversion coating treatment for AZ91 magnesium alloys by a permanganate-REMS bath [J]. Materials Corrosion, 2007, 58: 193−197.
[35] ZHELUDKEVICH M L, SALVADO I M, FERREIRA M G S. Sol−gel coatings for corrosion protection of metals [J]. Journal of Materials Chemistry, 2005, 15: 5099−5111.
[36] WANG D, BIERWAGEN G P. Sol-gel coatings on metals for corrosion protection [J]. Progress in Organic Coatings, 2009, 64: 327−338.
[37] TAN A L K, SOUTAR A M, ANNERGREN I F, LIU Y N. Multilayer sol-gel coatings for corrosion protection of magnesium [J]. Surface and Coatings Technology, 2005, 198: 478−482.
[38] MURILLO-GUTIERREZ N V, ANSART F, BONINO J P, MENU M J, GRESSIER M. Protection against corrosion of magnesium alloys with both conversion layer and sol–gel coating [J]. Surface and Coatings Technology, 2013, 232: 606−615.
[39] HU J, LI Q, ZHONG X, ZHANG L, CHEN B. Composite anticorrosion coatings for AZ91D magnesium alloy with molybdate conversion coating and silicon sol−gel coatings [J]. Progress in Organic Coatings, 2009, 66: 199−205.
[40] RUBIO F, RUBIO J, OTEO J L. A FT-IR study of the hydrolysis of tetraethylorthosilicate (TEOS) [J]. Spectroscopy Letters, 1998, 31: 199−219.
[41] SAPIC I M, BISTRICIC L, VOLOVSEK V, DANANIC V. Vibrational analysis of 3-Glycidoxypropyltrimethoxysilane polymer [J]. Macromolecular Symposia, 2014, 339: 122−129.

[42] SAPIC I M, BISTRICIC L, VOLOVSEK V, DANANIC V, FURIC K. DFT study of molecular structure and vibrations of 3-glycidoxypropyltrimethoxysilane [J]. Spectrochimica Acta Part A, 2009, 72: 833−840.
[43] SHI H, LIU F, HAN E H. Corrosion protection of AZ91D magnesium alloy with sol−gel coating containing 2-methyl piperidine [J]. Progress in Organic Coatings, 2009, 66: 183−191.
[44] YEKEHTAZ M, SITTNER F, UGAS-CARRION R, FLEGE S, BROTZ J, ENSINGER W. Characterization of protective sol–gel coatings on magnesium based on phenyltriethoxysilane precursor [J]. Thin Solid Films, 2010, 518: 5223−5226.
[45] PEBERE N, RIERA C, DABOSI F. Investigation of magnesium corrosion in aerated sodium sulfate solution by electrochemical impedance spectroscopy [J]. Electrochimica Acta, 1990, 35: 555−561.
[46] CHEN J, WANG J, HAN E, DONG J, KE W. Corrosion behavior of AZ91D magnesium alloy in sodium sulfate solution [J]. Materials Corrosion, 2005, 57: 789−793.
[47] CAI J, CAO F, CHANG L, ZHENG J, ZHANG J, CAO C. The preparation and corrosion behaviors of MAO coating on AZ91D with rare earth conversion precursor film [J]. Applied Surface Science, 2011, 257: 3804−3811.
[48] GURTEN A A, KELES H, BAYOL E, KANDEMIRLI F. The effect of temperature and concentration on the inhibition of acid corrosion of carbon steel by newly synthesized Schiff base [J]. Journal of Industrial and Engineering Chemistry, 2015, 27: 68−78.
[49] FURUI M, EBATA Y, YAMADA H, IKENO S, SAKAKIBARA K, SAIKAWA S. Grain boundary and intragranular reactions during aging in Mg−Al system alloys poured into sand and iron molds [J]. Materials Transactions, 2011, 52: 285−291.
[50] CURIONI M. The behaviour of magnesium during free corrosion and potentiodynamic polarization investigated by real-time hydrogen measurement and optical imaging [J]. Electrochimica Acta, 2014, 120: 284−292.

AM60B 镁合金防腐蚀 Ce−V/溶胶−凝胶复合涂层的应用

S. NEZAMDOUST, D. SEIFZADEH

Physical Chemistry Research Laboratory, Applied Chemistry Department,
Faculty of Basic Science, University of Mohaghegh Ardabili, Ardabil 5619911367, Iran

摘　要：研究 AM60B 镁合金表面复合涂层的应用，该涂层由铈−钒转化膜和混合溶胶−凝胶层组成。扫描电镜和 X 射线能谱分析显示铈−钒转化膜存在开裂结节结构，该转化膜由氧、铈、钒和镁原子组成。转化膜中的裂纹被致密无缺陷的混合溶胶−凝胶薄膜密封。在 Harrison 溶液中进行电位极化和电化学阻抗测试，结果表明铈−钒转化膜对镁合金提供了很小的防腐保护，然而复合涂层显著增大了镁合金的抗腐蚀性。通过密封铈−钒转化膜的裂缝，溶胶−凝胶膜对合金防护和阻碍腐蚀起到了很大的作用。极化测试后采用扫描电子显微镜验证了电化学测试结果。

关键词：镁合金；腐蚀；转化膜；溶胶−凝胶

(Edited by Xiang-qun LI)